Physics and Chemistry of the Earth: Part B, bf 25, 1285–1288.

Lightning and microphysics in a EULINOX supercell storm

Nikolai Dotzek [1], Hartmut Höller [1], and Claire Théry [2]

[1] DLR–Institut für Physik der Atmosphäre,
Oberpfaffenhofen, D–82234 Wessling, Germany

[2] ONERA–DMPH,
BP 72–29, F–92322 Châtillon Cedex, France

Proc. 1st European Conference on Radar Meteorology

Received 15 June 2000, in final form 15 July 2000

Corresponding author's address:
Dr. N. Dotzek
DLR–Institut für Physik der Atmosphäre,
Oberpfaffenhofen, D–82234 Wessling, Germany.
E–mail: Nikolai.Dotzek@dlr.de,
Tel: +49–8153–28–1845, Fax: +49–8153–28–1841.

Physics and Chemistry of the Earth: Part B, bf 25, 1285–1288.

Lightning and microphysics in a EULINOX supercell storm

Nikolai Dotzek [1], Hartmut Höller [1], and Claire Théry [2]

[1] DLR–Institut für Physik der Atmosphäre,
Oberpfaffenhofen, D–82234 Wessling, Germany

[2] ONERA–DMPH,
BP 72–29, F–92322 Châtillon Cedex, France

Received 15 Jun 2000, in final form 15 July 2000

Abstract

A combined analysis of data from a C–band polarization diversity Doppler radar and a 3D VHF interferometric lightning mapping system is presented for the 21 July 1998 EULINOX supercell thunderstorm. Its lower positive charge center emitted much more VHF radiation than expected from the well–known tripole concept. In higher cloud regions VHF activity was sometimes linked to distinct levels, but their height varied strongly within the Cb–cell during its evolution. In early stages the supercell showed moderate VHF activity in reflectivity regions near 30 dBZ. In later stages VHF activity rose considerably and was linked to higher reflectivity factors of 40 to 50 dBZ.

1 Introduction

The two–year **Eu**ropean **li**ghtning **n**itrogen **ox**ides project (EULINOX) mainly aimed at an improved understanding of NO_X production within central European thunderstorms. During the intensive observation period in summer 1998 a great variety of analysis methods were applied: aside from aircraft measurements of chemical constituents within and around thunderclouds, interferometric measurements of VHF sources from lightning discharges in two and three dimensions were made by the ONERA and compared to those of a two–dimensional LPATS (Lightning Positioning and Tracking System) network.

The ONERA interferometric lightning mapper (ITF) consisted of two VHF interferometric stations 40 km apart, each at 25 km distance from the operational center in Oberpfaffenhofen. Lightning flashes, either intracloud or cloud–to–ground, emit strongly in the VHF band, and each interferometric station detects this radiation in a narrow band (1 MHz width) at 114 MHz and records its amplitude and direction of arrival with a 23 μs sampling rate. The ITF mapping system can detect the negative leaders and high current discharges (intracloud recoil streamers, cloud–to–ground dart leaders and return strokes) all along their propagation paths. Both stations give the azimuth of the VHF sources, and the three-dimensional (southern) station can also measure the elevation of the sources. The x,y–position of a source is determined from the azimuthal directions relative to the two stations and the elevation then allows to retrieve the altitude of the source. VHF sources are then associated in "bursts", which correspond to individual discharges, and bursts are grouped into flashes. We must note that the accuracy of the elevation sensor decreases rapidly for very low (below 5°) and very high (above 48°) elevations. Therefore, a storm can be fully observed from 2 km AGL up to 11 km if it is within 10 km and 25 km distance from the southern interferometric station.

The C–band polarimetric Doppler radar POLDIRAD at DLR in Oberpfaffenhofen provided three–dimensional information on the storm's dynamical and microphysical structure and allowed for an identification of the different hydrometeor types in the thundercloud and the accompanying anvil region. The present combination of data from ONERA's VHF interferometric lightning mapper and DLR's polarization diversity radar provided a detailed view on the evolution of the lightning activity and its relation to cloud microphysics and dynamics in space and time:

- identification of main lightning activity regions inside the cloud compared to theoretical predictions,
- correlations between lightning discharges and certain radar parameters, such as the reflectivity factor,
- trends in these findings during cloud evolution.

The paper is organized as follows: Sec. 2 briefly reviews the life–cycle of the supercell storm before in Sec. 3 the vertical distribution of VHF activity due to lightning flashes is described. The relation between electrical activity and radar reflectivity is treated in Sec. 4. The Secs. 5 and 6 present discussion and conclusions.

2 Life cycle of the supercell storm

The EULINOX supercell storm of 21 July 1998 (Höller et al., 1999, 2000, this volume) was the right–mover of a storm splitting at about 1645 UTC over the Allgäu region in southern Germany. While the left–moving cells decayed very soon, the right–moving cell (heading in an easterly direction within the mid–level flow from south–west) intensified very rapidly and developed radar–detectable supercell characteristics such as a single persistent precipitation core, a bounded weak echo region, an echo overhang, and mesocyclonic rotation.

After 1700 UTC the young supercell storm approached the experimental area of approximately 60 km radius around Oberpfaffenhofen. Fig. 1 shows the flash rate per minute measured by the ITF sensor, both for the whole area (solid line) and the region of the supercell alone (lower filled curve). While there was considerable thunderstorm activity in the area before the supercell originated from its parent storm, we focus on the time period 1700–2000 UTC which contains the intensification phase (up to 1800 UTC), the mature stage (up to 1830 UTC) and the subsequent decay of the storm into a multicellular complex. Coincidentally, the supercell passed right over the 3D ITF–station between about 1800–1815 UTC, already slightly weakening. We see from Fig. 1 that the supercell flash rate during the most vigorous phase of the storm exceeded 40 min^{-1} and hardly fell below 30 min^{-1}. Note the rapid rise of the flash rate after 1730 UTC and the minimum around 1815 UTC, which is likely caused by the storm's passage over the ITF sensor (revealed by radar and LPATS observations) and not due to a genuine decrease of lightning activity.

Radar observations showed that the most noticeable cloud growth and internal organization took place from 1730 UTC to 1800 UTC, accompanied by the large rise in flash rate. The storm was tracked by POLDIRAD sector volume scans repeated roughly every 3 minutes and additional two–dimensional range–height- and plan position indicator scans. The radar–observed echo tops (cf. Höller et al., 2000, this volume) are depicted by the numbers in Fig. 1 from 1730 to 1833 UTC. The Cb–system lost its supercell structure after about 1845 UTC and then was better characterized as a multicellular storm with some phases of reintensification due to the development of new cells.

3 Vertical structure of VHF activity

Theoretical and experimental results indicate the presence of a negative charge center around the $T = -15° \pm 10°$ C level and an upper positive charge center near the $T = -35° \pm 10°$ C level within mature Cb–clouds. A smaller lower positive charge region can sometimes be found close to the freezing level. This three–level conceptual model is known as the tripole model of thunderstorm electrification (Williams, 1989; Saunders, 1993). On 21 July 1998 the heights of these temperature levels were deduced from a composite afternoon vertical sounding from radiosonde, aircraft, dropsonde and mesonet data. The height of a negative charge center can be expected to be within 5 and 7.5 km AGL, and an upper positive charge center approximately 3 km higher up, i. e. at a height of about 8 to 10 km AGL. These regions are indicated in Fig. 2 by the hatched areas. The freezing level was at about 3.5 km AGL.

Within the evaluation area ranging between 10 km and 25 km around the 3D ITF station Wielenbach vertical profiles of VHF sources integrated over 3 min intervals and a cubic 1 km^3 grid (chosen to coincide roughly with the radar scan volume and time interval) have been analyzed for the presence of peak levels. This spatial resolution is comparable both to radar and mesoscale model data (cf. Höller et al., 2000, this volume). During the time period considered (1700 to 2000 UTC), most vertical profiles for which distinct peaks could be identified were single–peak profiles (666 cases). In another 204 cases two peaks were found. Then one and two–peak profiles were averaged separately. The dashed line in Fig. 2 gives the average of all one–peak profiles and the solid line the average of the two–peak profiles. In both cases a low–level maximum at 3.5 km height is most pronounced. The solid curve, however, shows a secondary maximum at 6.5 km AGL which corresponds to the –15° C level of 21 July 1998. Yet in neither of the average profiles do we find an upper–level maximum near the –30° C region inside the cloud where we would expect the main positive charge level of a Cb–tripole. There are VHF sources at that level, but not enough to form a distinguishable peak.

To resolve the temporal trend in the height of these levels and to give an impression of their variability Fig. 3 shows the time–height series of the peaks in the 666 single- (a) and the 204 double–peak profiles (b). Especially for profiles with one maximum there is a large variation of the maximum's height even in the rather small evaluation area considered here. The single maximum can be found practically anywhere in the Cb–cloud although most profiles peak near the freezing level. Similar arguments apply for Fig. 3 b. Note the large scatter between about

1800 and 1815 UTC when the supercell passed overhead the 3D–ITF sensor and made 3D reconstruction difficult, and also the significant minimum of the observed level heights around 1845 UTC. This corresponds to a time at which the supercell had mostly decayed while new (multicellular) activity had not yet formed again. We may state that active cells with strong updrafts lead to a rise of the zones with maximum VHF emissions.

4 Synthesis of ITF and radar data

For a discussion of lightning and polarimetric radar parameters in this storm cf. Höller et al. (2000, this volume). Here we address the most basic radar–derived quantity, the reflectivity factor Z.

In the EULINOX storm the region of high VHF activity typically was shifted away from the reflectivity core of the supercell storm. The shift was mostly to the left downshear side of the storm's center, i. e. on the northern flank of the east–moving storm (Dotzek et al., 2000). To obtain information on the correlation between number of VHF sources N_{VHF} and reflectivity factor Z, the volume data measured by the radar at 1730, 1745, 1757, 1809, 1821, and 1833 UTC were related to the total number of VHF sources within 3 min periods starting at the six given volume scan times. As the radar data were interpolated onto the same 1 km^3 grid as used for the ITF data, the points could directly be analyzed from a scatter diagram of N_{VHF} versus Z.

This is shown in Fig. 4 a for the growing phase of the storm (1730, 1745, squares) and in Fig. 4 b for its early decaying stage (1821, 1833, crosses). In all four volume scans the highest observed reflectivities interpolated to the cartesian 1 km^3 grid were in the range from 50 to 52.5 dBZ. In the developing stage of the storm, no VHF data points are found for Z $\geq$ 43 dBZ. Instead, weak VHF activity is found with usually less than 10 VHF sources per 3 min interval and per km^3. The peak of the scattered points is located at roughly 32 dBZ. The number of sources decreases slower towards lower reflectivity factors than to higher dBZ–values. This skewness towards the higher values of Z is also found during the decaying stage of the storm in Fig. 4 b. But now the reflectivity in grid boxes with VHF sources extends up to about 52 dBZ and the VHF activity itself also has increased substantially: many grid boxes contain 10 or more sources per 3 min interval and per km^3 with a peak value of 30. In addition the location of this maximum has shifted towards higher reflectivity factors. Instead of 32 dBZ in the early stage, the scatter plot now peaks at 45 dBZ and then drops off very rapidly with increasing Z. The

data are more strongly skewed than before, but in general the shapes of the two scatter–data sets seem to bear a similarity, because the points from Fig. 4 a roughly group within the left flank of the data region of Fig. 4 b. As a consequence, for $Z < 25$ dBZ the number of VHF signals is always less than 5 per km^3 and 3 min interval.

5 Discussion

For the vertical structure of lightning VHF activity our results indicate that in some parts of the cloud VHF signatures showing a preference for one or two levels of high activity appeared to be present. However, other parts of the cloud showed a large vertical variability of enhanced VHF emissions. Following Rust & Marshall (1996) we can state here that the real structure of thunderstorms is far more complex than the simple tripole concept, even though the physical processes leading to the tripole are likely to be present in some parts of the thundercloud.

The strong VHF activity near the freezing level within this supercell storm remains an open issue. On the one hand this would indicate that the lower (secondary) positive charge layer of the Cb–cloud was overwhelmingly active in this special case. Physical evidence for this assumption is given by Williams (1989) and Saunders (1993) as well as in a different context by Shepherd et al. (1996) who also observed strong electric fields and charges near the melting layer in the stratiform part of mesoscale convective systems. The authors argue that a melting–charging mechanism could be responsible for that.

On the other hand the low–level negative leaders which were found in the data from the EULINOX supercell are likely to be highly prominent in VHF due to the larger air pressure at this low altitude (Lalande & Bondiou–Clergerie, 1997). Thus they tend to enhance the VHF signatures of lightning activity there. Future analysis of other EULINOX storms of different type will further clarify the processes that govern cloud electricity near the freezing level.

6 Conclusions

Our analysis of the radar and ITF data recorded during the 21 July 1998 EULINOX supercell leads us to conclude:

1. cloud–scale aspects of thunderstorm electricity can effectively be studied by combining radar and VHF interferometric lightning mapper data,

2. only in parts of the Cb–cloud VHF signals were linked to certain persistent height regions,

3. the heights of large VHF emissions follow the evolution of the cloud — higher up during cloud growth, lower during and after decay,

4. a strong lower positive charge center near 0° C was observed in this supercellular storm,

5. with proceeding storm evolution, VHF activity becomes more intense and is linked to increasing values of Z.

Acknowledgments

This work was partly funded by the Commission of the European Communities under contract No. ENV4–CT97–0409.

References

Dotzek, N., H. Höller, C. Théry, 2000: VHF–interferometry and radar observation: Implications for nitrogen oxides production. *EULINOX — final report*, European commission, Luxembourg, 224 pp.

Höller, H., P. Laroche, M. Hagen, J. Seltmann, U. Finke, 1999: Radar and lightning structures of thunderstorms during EULINOX. *Proc. 29th Conf. on Radar Meteorol.*, Montreal, 611–612.

Höller, H., T. Fehr, C. Théry, J. Seltmann, H. Huntrieser, 2000: Radar, lightning, airborne observations, and modelling of a supercell storm during EULINOX. *Phys. Chem. of the Earth: Part B*, this volume.

Lalande, P., A. Bondiou–Clergerie, 1997: Collection and analysis of available in–flight measurement of lightning strikes to aircraft. *Final report of Fulmen European Project on Analysis of Experimental data and models for upgraded lightning protection requirements*, DG VII, Transport Research and Technological Development Programs. Rep. Al–95–SC.204–RE / 210–D:1.

Rust, W. D., T. C. Marshall, 1996: On abandoning the thunderstorm tripole–charge paradigm. *J. Geophys. Res.* **101**D, 23499–23504.

Saunders, C. P. R., 1993: A review of thunderstorm electrification processes. *J. Appl. Meteorol.* **32**, 642–655.

Shepherd, T. R., W. D. Rust, T. C. Marshall, 1996: Electric fields and charges near 0° C in stratiform clouds. *Mon. Wea. Rev.* **124**, 919–938.

Williams, E. R., 1989: The tripole structure of thunderstorms. *J. Geophys. Res.* **94**D, 13151–13167.

Figure captions

Figure 1: Flash rate for the supercell (filled) and the total observation area (solid) in the time period 1530–2200 UTC measured by the ITF sensor. The numbers atop the curves give the supercell radar echo top in km AGL.

Figure 2: Average (1700–2000 UTC) vertical VHF profiles of 666 columns containing one distinct maximum (dashed) and 204 columns containing two maxima (solid). The hatched height ranges mark probable locations of main charge layers on 21 July 1998.

Figure 3: Time series from 1700–2000 UTC showing the height of the maxima for the one–peak profiles (a) and the two–peak profiles (b) of Fig. 2. The symbol $\diamond$ denotes the height of the lower, and $+$ the height of the upper–level VHF maximum.

Figure 4: Scatter plot between number of VHF sources per 3 min interval km^{-3} and radar reflectivity factor Z for 1730, 1745 UTC (a, squares) and 1821, 1833 UTC (b, crosses).

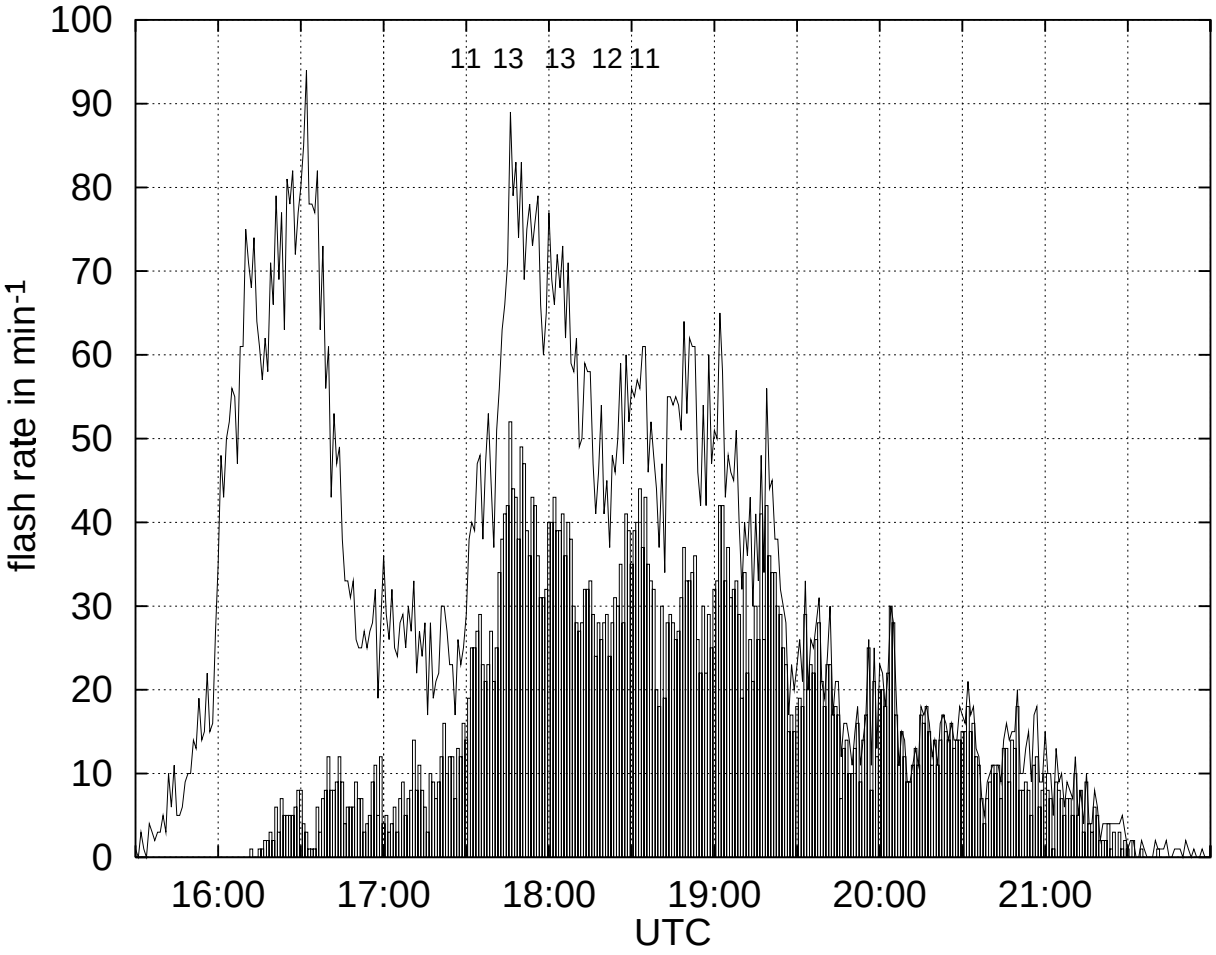
11 13 13 12 11
flash rate in min-1
UTC
0
10
20
30
40
50
60
70
80
90
100
16:00
17:00
18:00
19:00
20:00
21:00

Figure 1

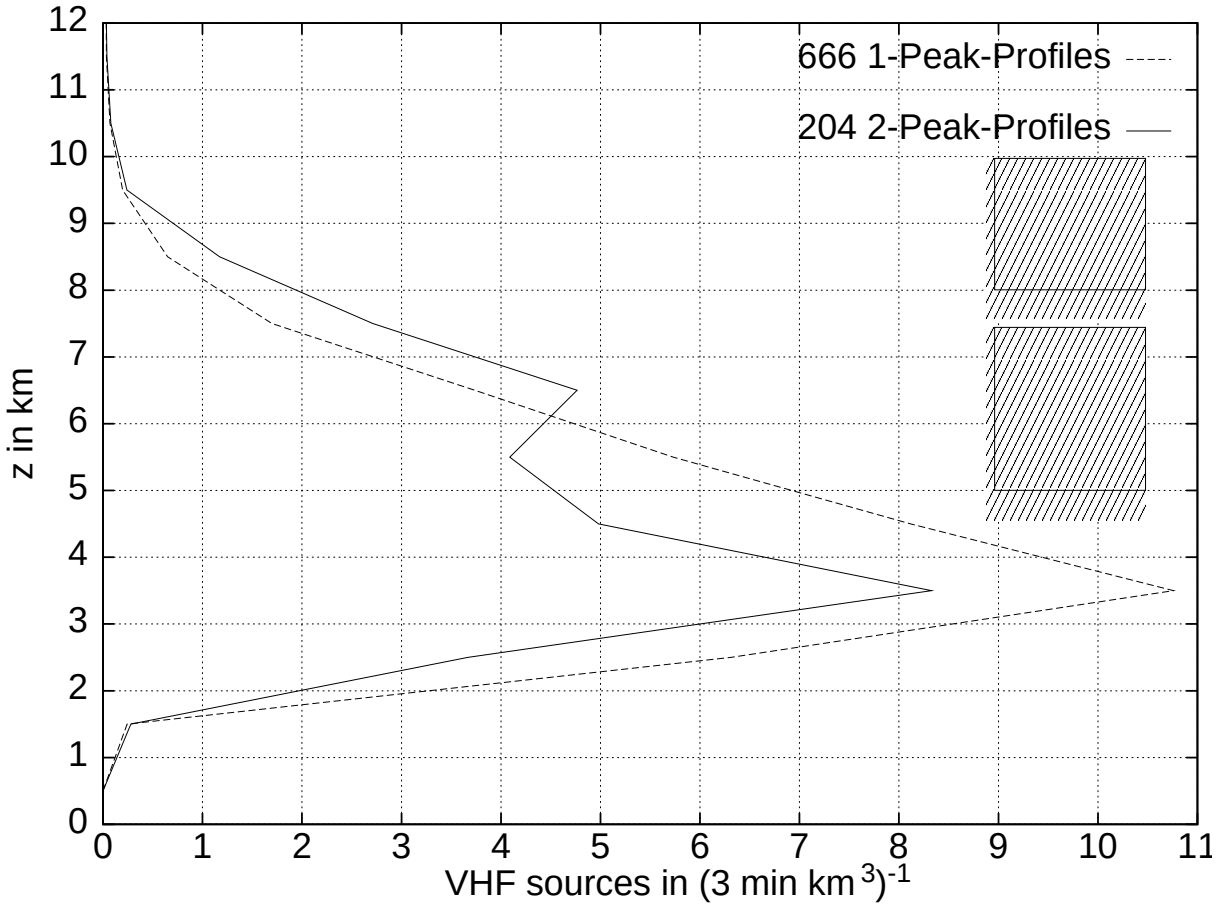
666 1-Peak-Profiles
204 2-Peak-Profiles
z in km
VHF sources in (3 min km 3)-1
0
1
2
3
4
5
6
7
8
9
10
11
12

Figure 2

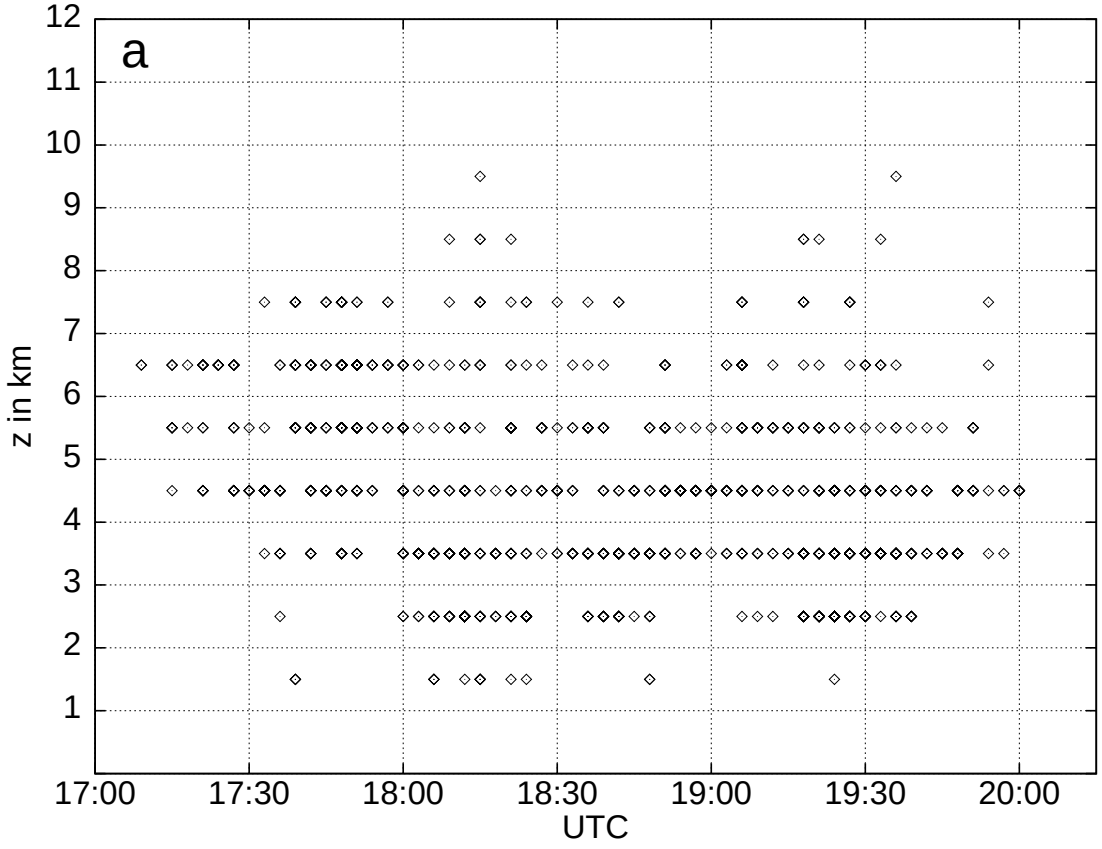
a
z in km
UTC
17:00
17:30
18:00
18:30
19:00
19:30
20:00
1
2
3
4
5
6
7
8
9
10
11
12

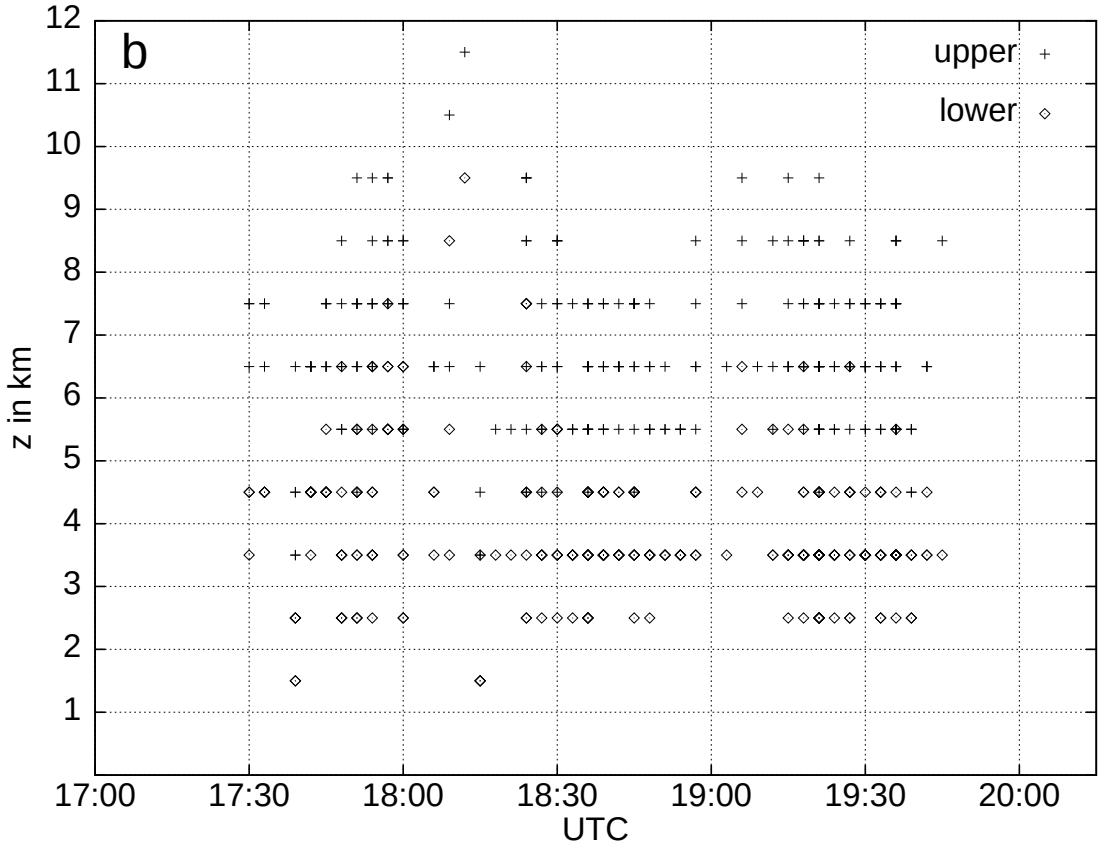
b
upper
lower
z in km
UTC
17:00
17:30
18:00
18:30
19:00
19:30
20:00
1
2
3
4
5
6
7
8
9
10
11
12

Figure 3

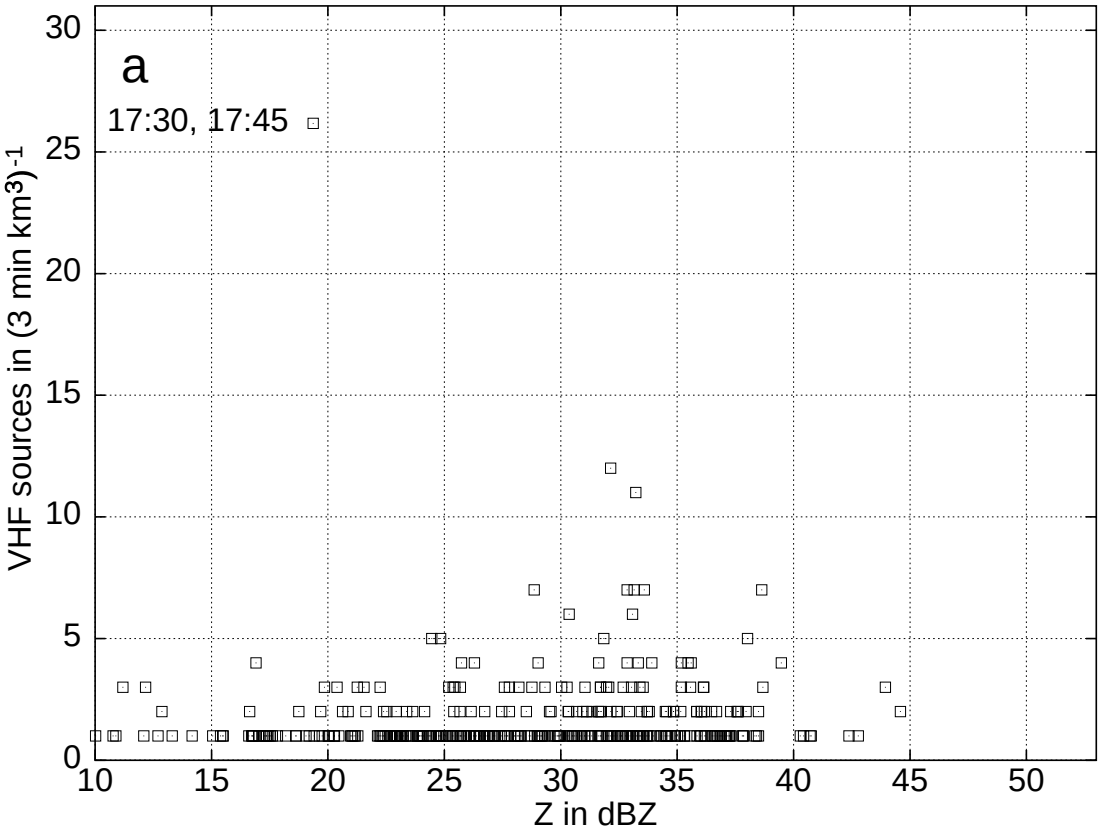
a
17:30, 17:45
VHF sources in (3 min km³)⁻¹
Z in dBZ
0
5
10
15
20
25
30
10
15
20
25
30
35
40
45
50

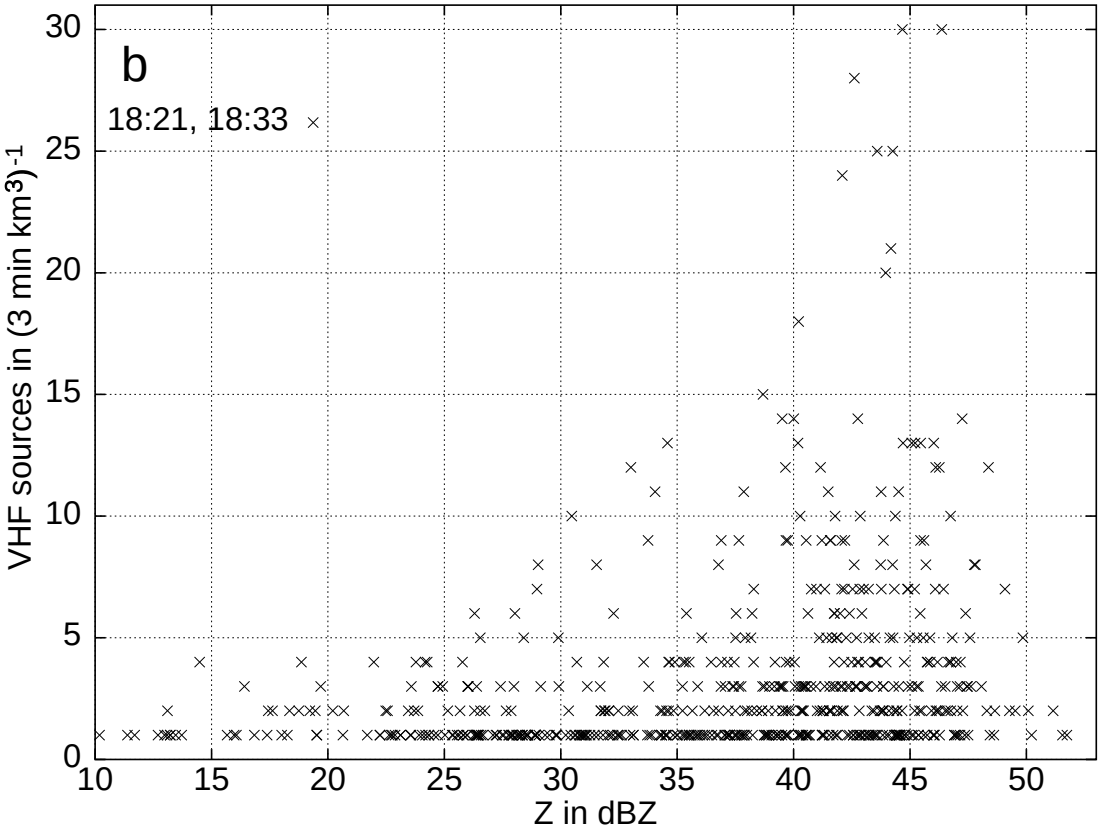
b
18:21, 18:33
VHF sources in (3 min km³)⁻¹
Z in dBZ
0
5
10
15
20
25
30
10
15
20
25
30
35
40
45
50

Figure 4